



Supplemental Material for
Internal Variability and Regional Climate Trends in an Observational Large Ensemble

Karen A. McKinnon and Clara Deser

Climate and Global Dynamics Division, National Center for Atmospheric Research, Boulder, Colorado

[© Copyright 2018 American Meteorological Society](#)

Permission to use figures, tables, and brief excerpts from this work in scientific and educational works is hereby granted provided that the source is acknowledged. Any use of material in this work that is determined to be “fair use” under Section 107 of the U.S. Copyright Act or that satisfies the conditions specified in Section 108 of the U.S. Copyright Act (17 USC §108) does not require the AMS’s permission. Republication, systematic reproduction, posting in electronic form, such as on a website or in a searchable database, or other uses of this material, except as exempted by the above statement, requires written permission or a license from the AMS. All AMS journals and monograph publications are registered with the Copyright Clearance Center (<http://www.copyright.com>). Questions about permission to use materials for which AMS holds the copyright can also be directed to permissions@ametsoc.org. Additional details are provided in the AMS Copyright Policy statement, available on the AMS website (<http://www.ametsoc.org/CopyrightInformation>).

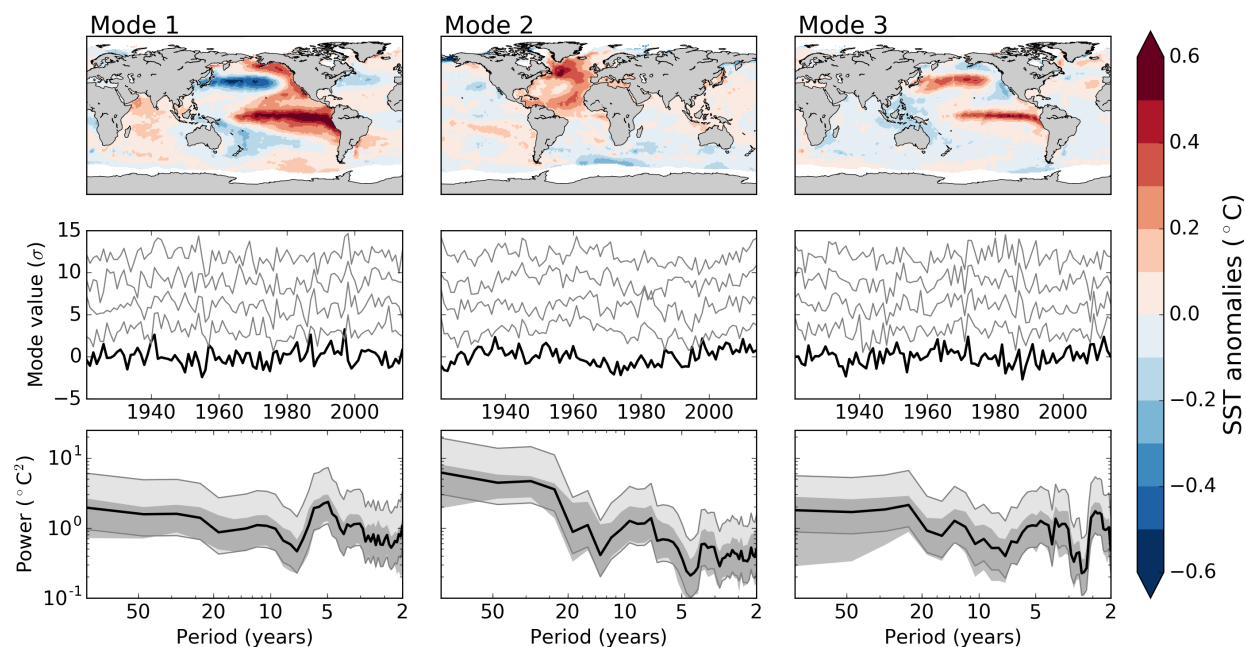


Figure S1: As in Fig. 1, but for JJA. The spatial pattern and temporal behavior of ENSO, PDO, and AMO, and their surrogates. Modes 1 and 3 collectively explain ENSO and PDO, while Mode 2 represents the AMO. **First row:** The sea surface temperature pattern associated with each mode. **Second row:** The time series of each mode (thick black line), and four example surrogates (thin gray lines). Each surrogate is offset in the vertical by three units for visual clarity. **Third row:** The power spectra of each mode (thick black line) and its 95% confidence interval (light gray shading, outlined by thin black lines). The 95% range of the spectra for the surrogate time series is shown in the dark gray shading. See text for details.

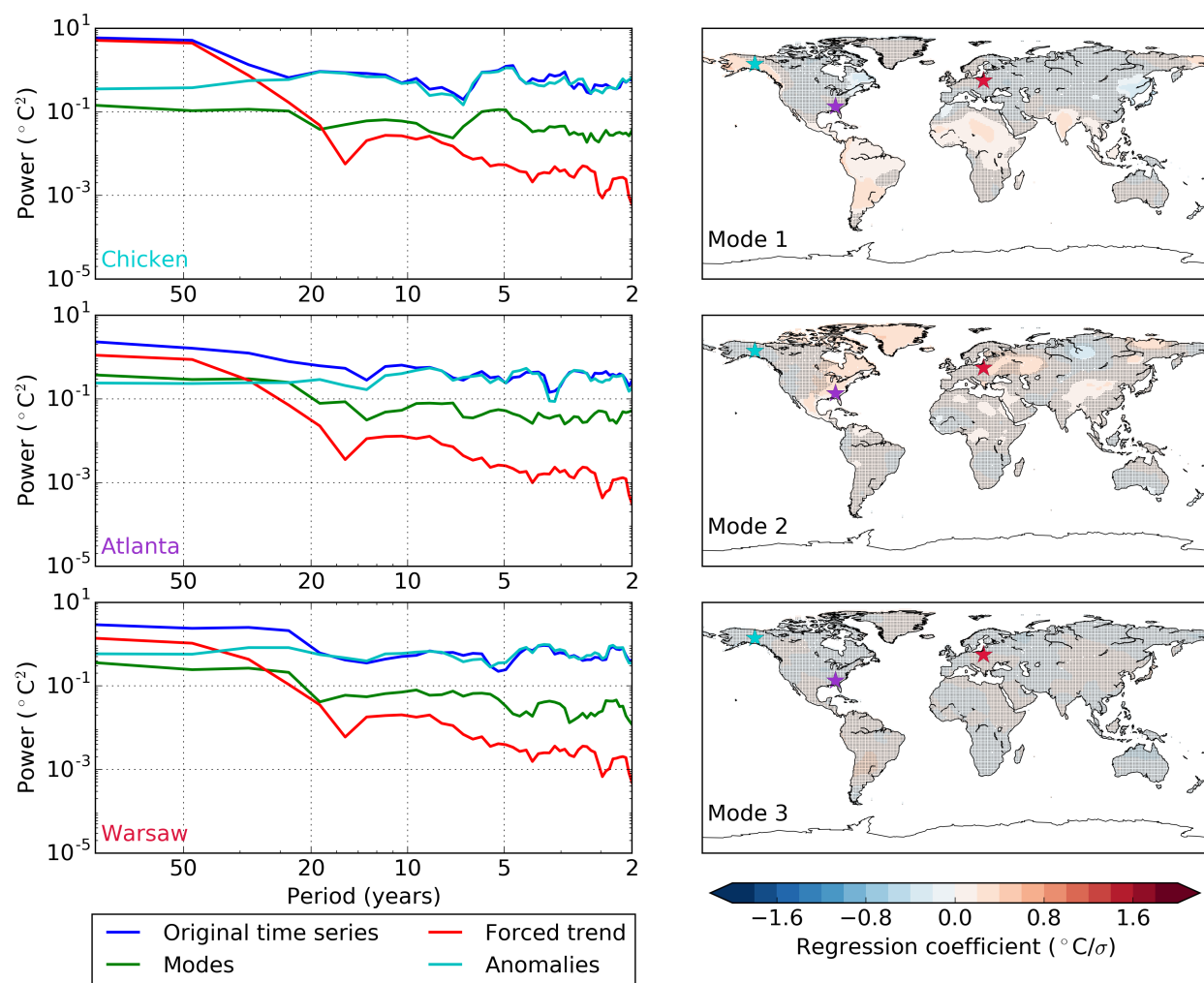


Figure S2: As in Fig. 2, but for JJA. Contribution of ENSO, PDO, and AMO to interannual DJF temperature variability estimated over 1921-2014. Modes 1 and 3 collectively explain ENSO and PDO, while Mode 2 represents the AMO. **Right column:** The sensitivity of JJA temperature to the three dominant SST modes (see Fig. S1) estimated via linear regression. Stippling indicates an insignificant relationship using a False Discovery Rate of 10%; p-values at each gridbox are estimated using a two-sided t-test. **Left column:** Power spectra for three representative gridboxes, indicated by the location of the stars in the maps. In all cases, there is a clear separation of timescales between the inferred forced trend (red) and the residual anomalies (teal).

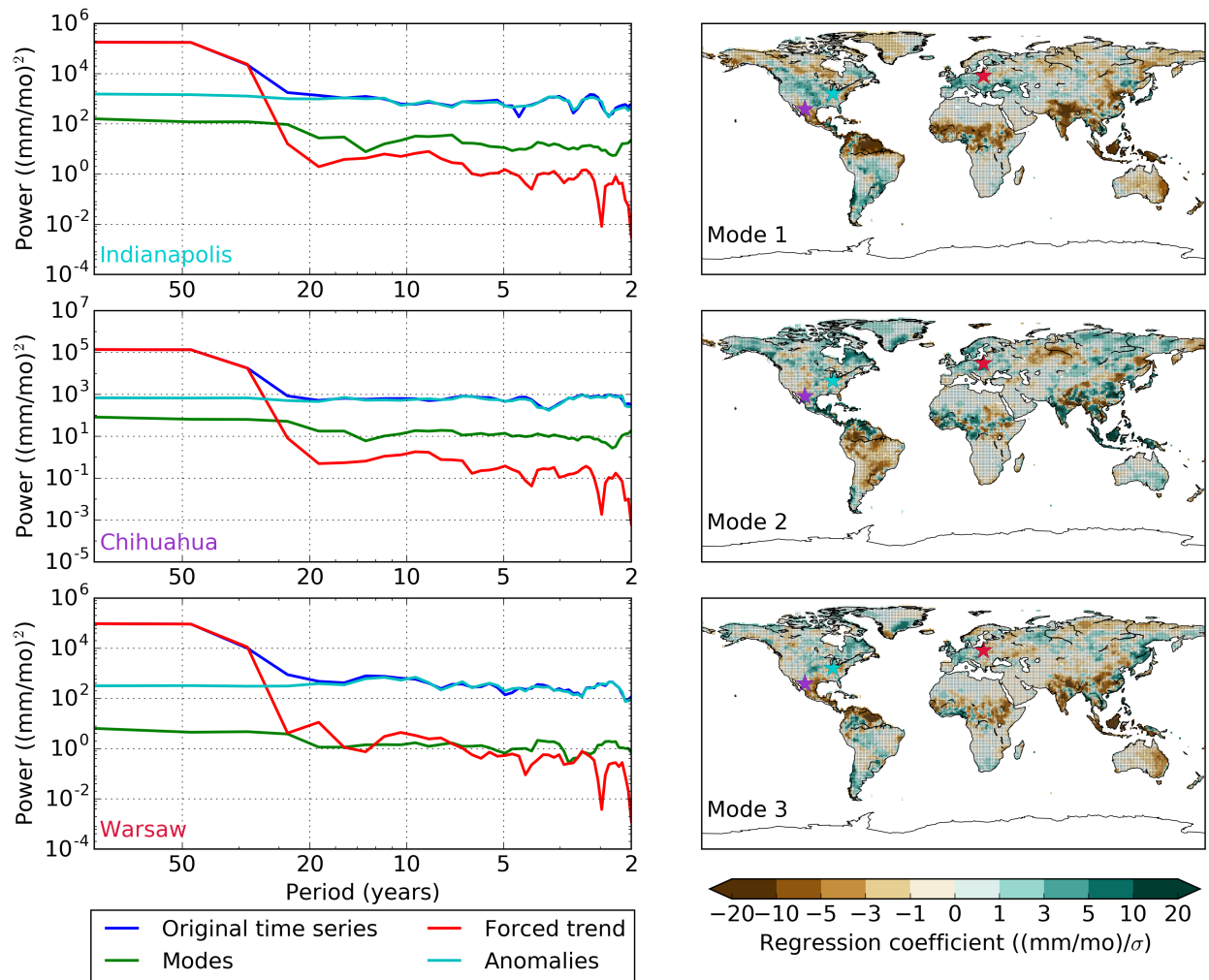


Figure S3: As in Fig. S2, but for precipitation.

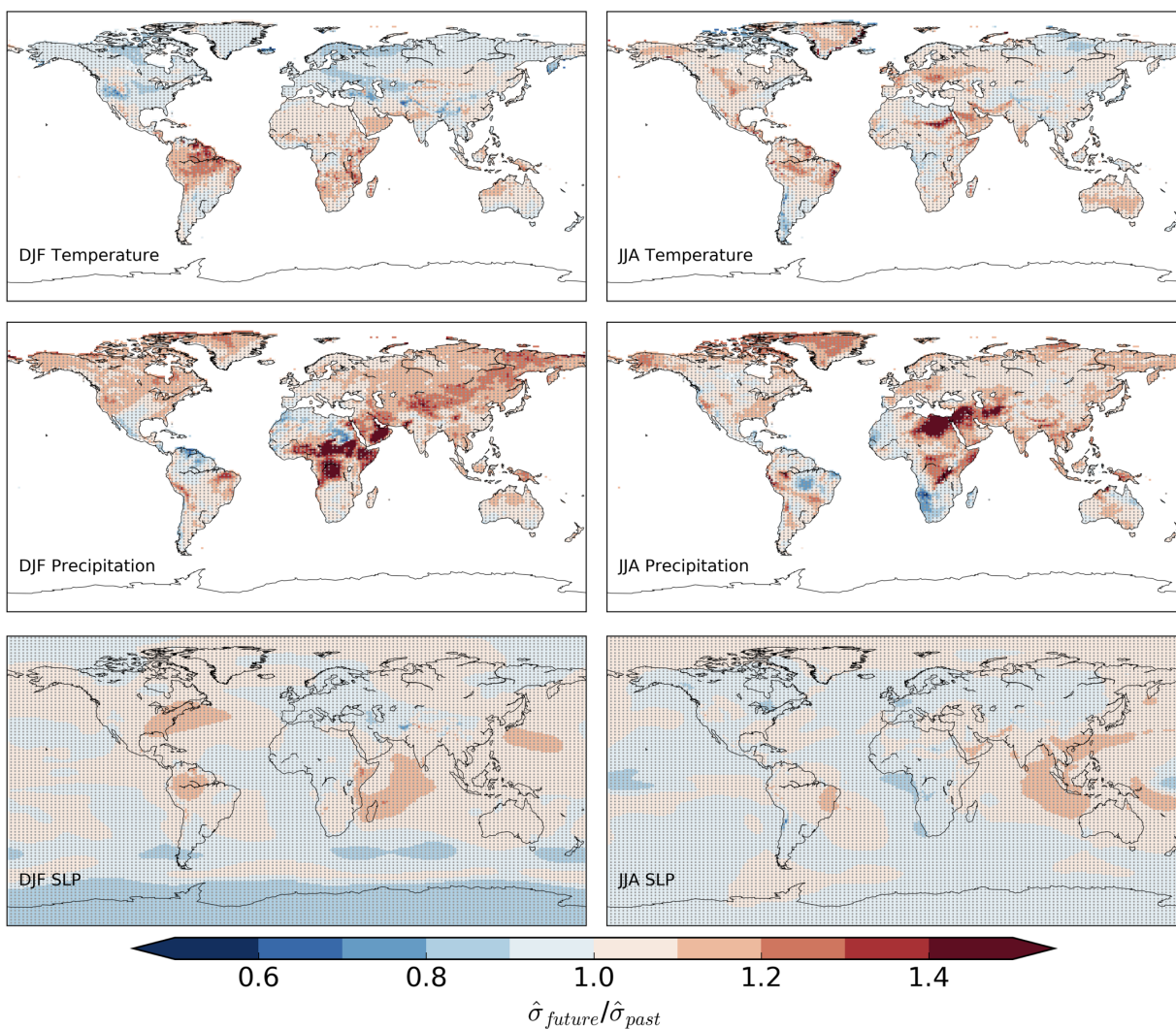


Figure S4: The ratio of interannual standard deviations of (top) temperature, (middle) precipitation, and (bottom) sea level pressure for (left) DJF and (right) JJA from the NCAR CESM1 Large Ensemble during 2015-2064 compared to 1965-2014. Interannual variability is estimated after first removing the ensemble mean, and estimates are pooled across the 40 ensemble members. Regions where there is an insignificant difference between the two periods are stippled. P-values at each gridbox are calculated using an F-test, and the field-wide significance is based on a False Discovery Rate of 10%.

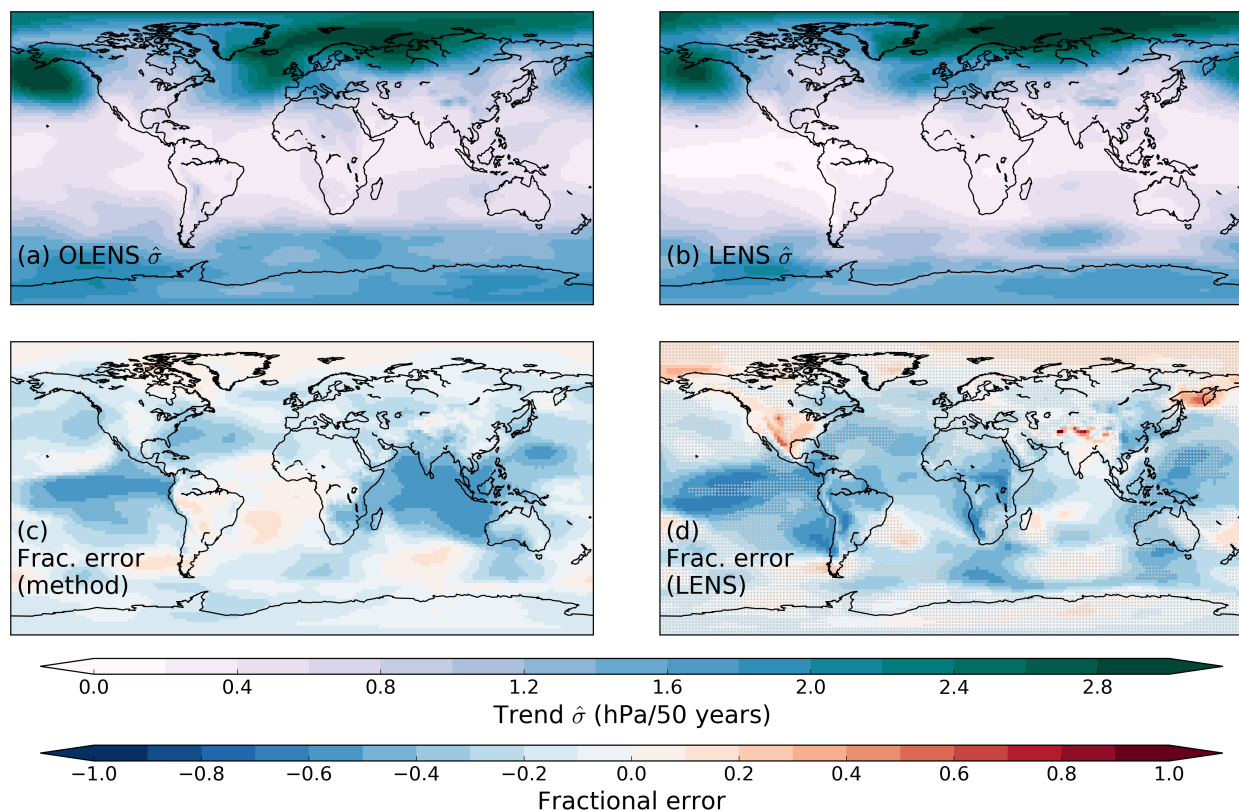


Figure S5: Trend variability in the Observational Large Ensemble (OLENS), the NCAR CESM1 Large Ensemble (LENS), and validation of the OLENS methodology for DJF sea level pressure (SLP). **(a)** The standard deviation of 50-year (1965-2014) linear SLP trends across the 1000 members of OLENS. **(b)** The standard deviation of 50-year linear SLP trends across the 40 members of LENS. **(c)** The fractional error of the bootstrapping methodology, estimated as the standard deviation of 50-year linear SLP trends in LENS minus the standard deviation of 50-year linear SLP trends estimated from bootstrapping members of LENS, normalized by the bootstrap-based estimate. **(d)** The fractional difference between LENS- and OLENS-based estimates of the standard deviation of 50-year linear SLP trends, i.e. $(a - b)/(b)$. Stippling indicates locations where the difference is insignificant using a False Discovery Rate of 10%; p-values are estimated at each gridbox as the probability that the difference between LENS and the bootstrapped observations could occur from bootstrapping individual members of LENS

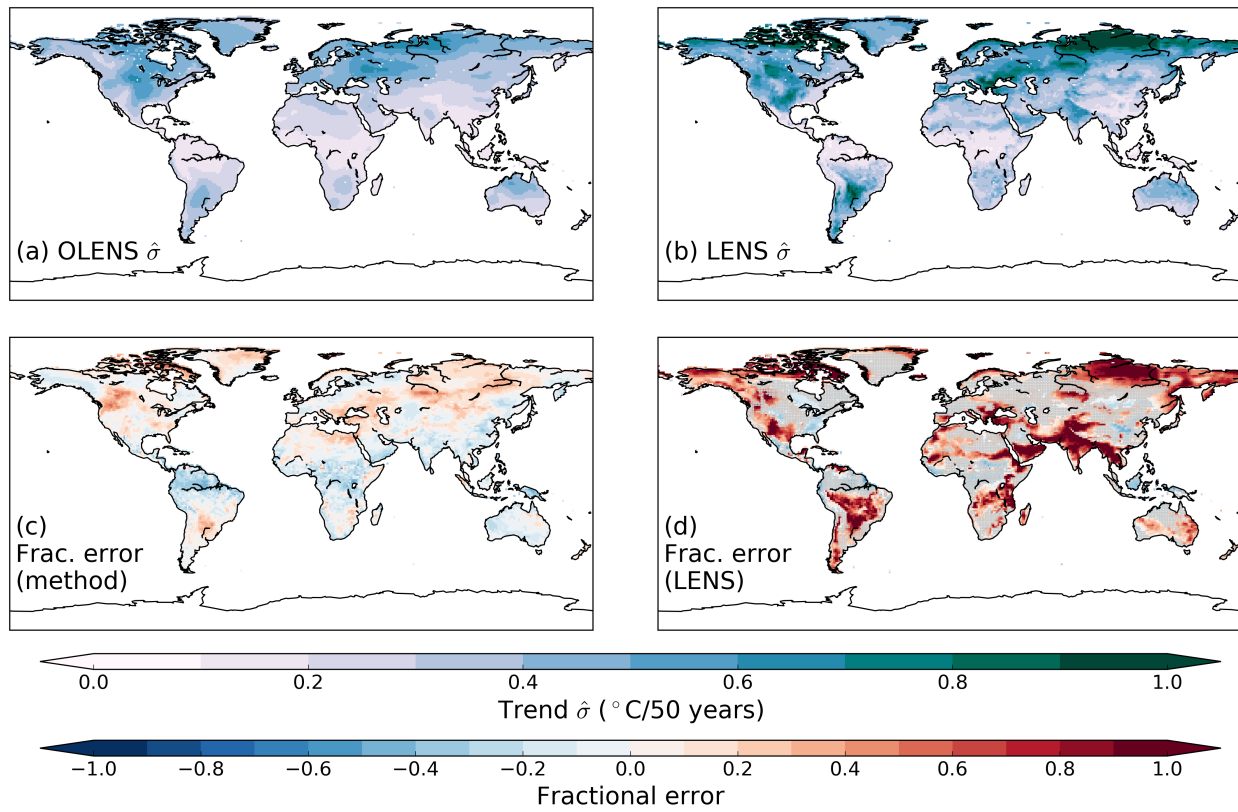


Figure S6: As in Fig. 4, but for JJA.

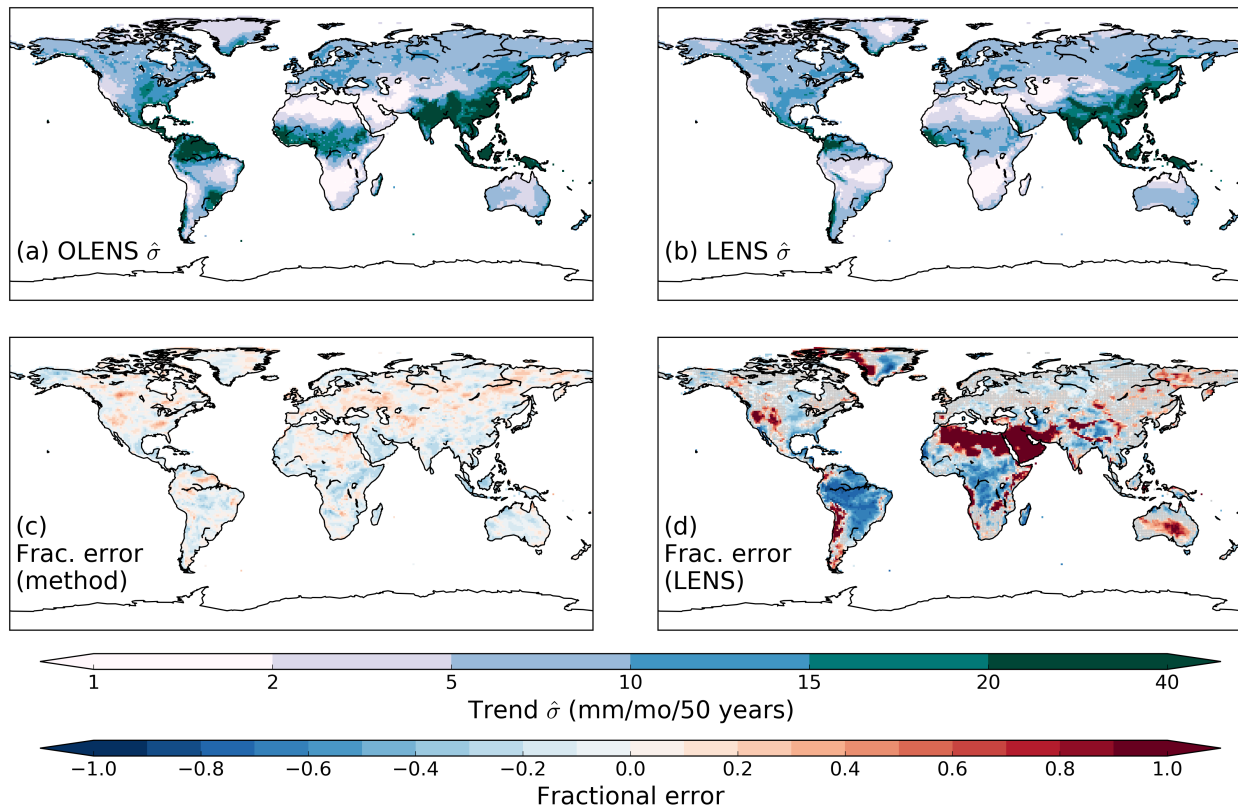


Figure S7: As in Fig. 5 but for JJA.

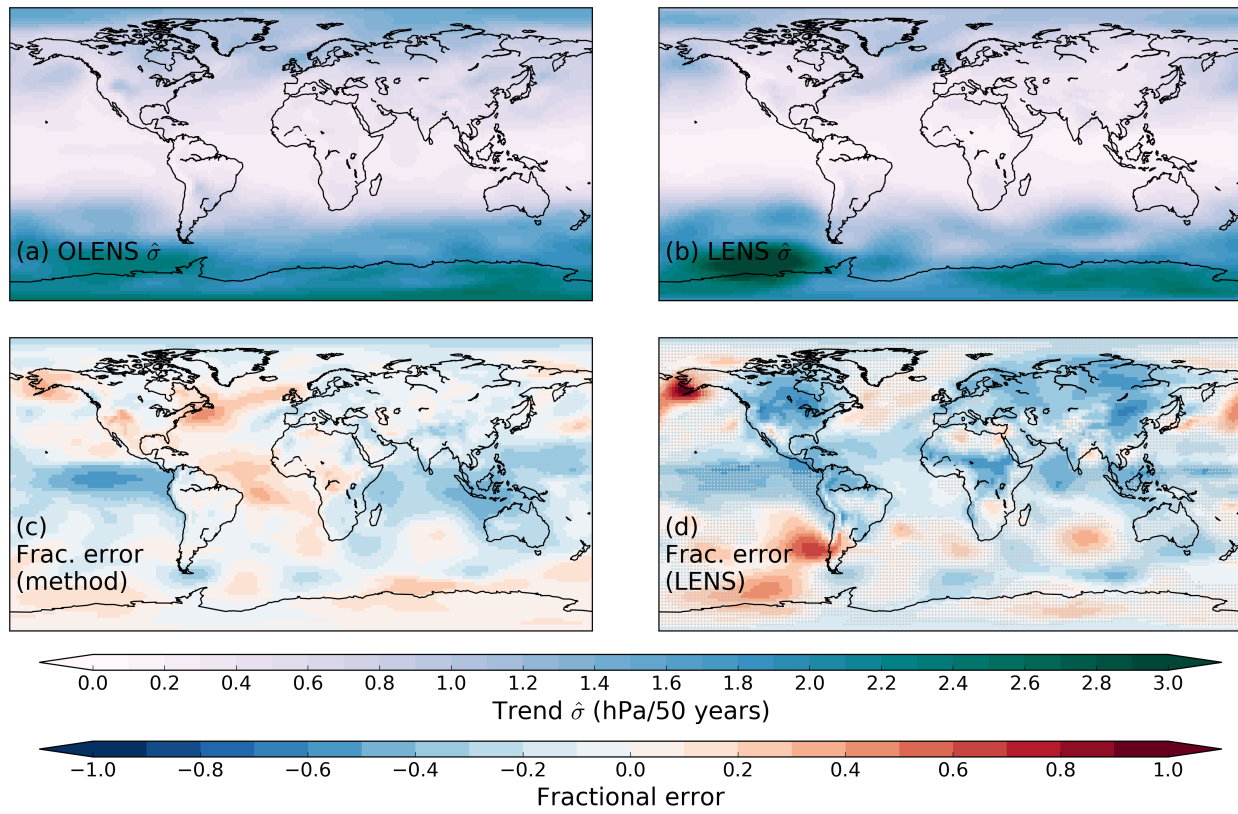


Figure S8: As in Fig. S5, but for JJA.

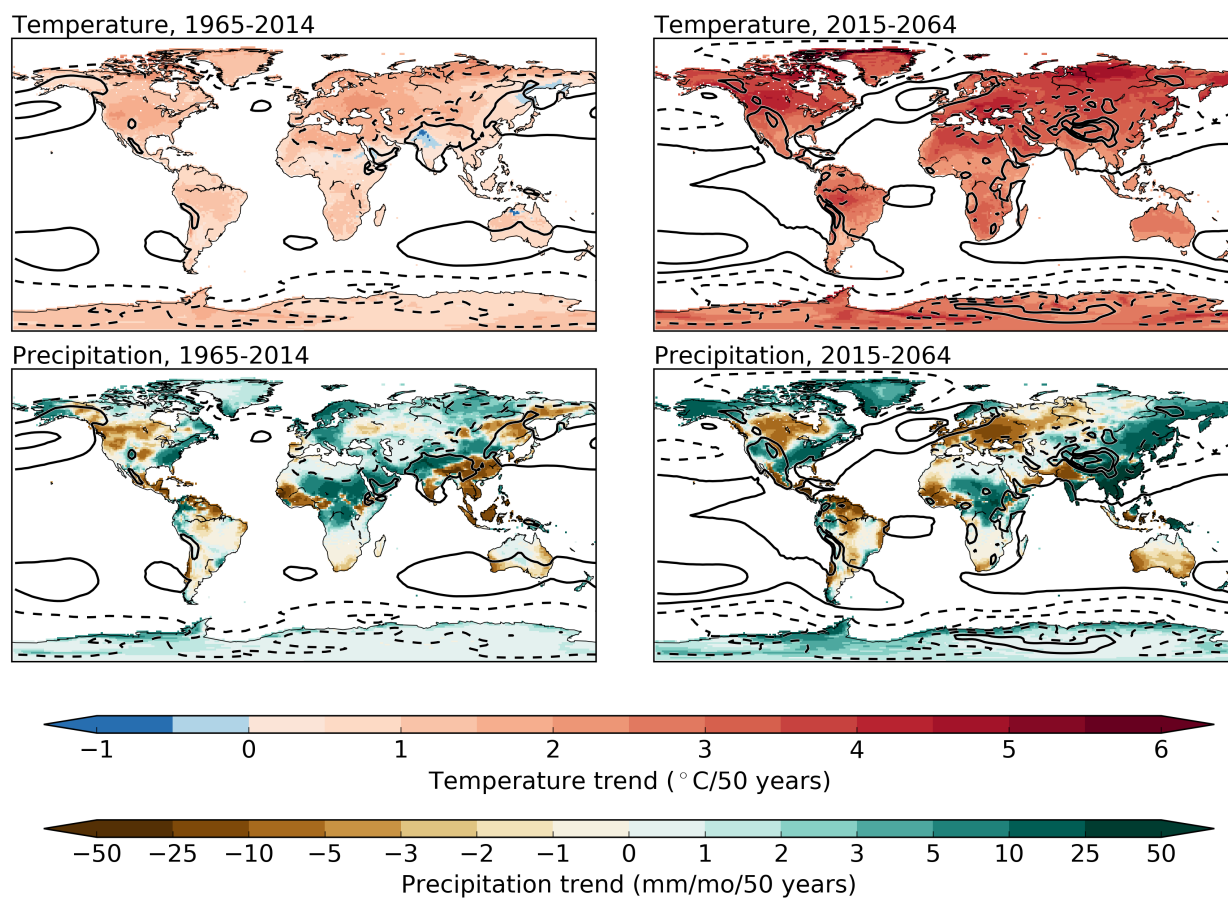


Figure S9: Ensemble-mean linear trends from the NCAR CESM1 Large Ensemble (LENS) in JJA temperature (top row) and precipitation (bottom row) for the past (left column, 1965-2014) and next (right column, 2015-2064) 50 years. Trends in SLP are indicated by contours, with a contour interval of 1hPa/50 years, beginning with contours of ± 0.5 hPa/50 years.

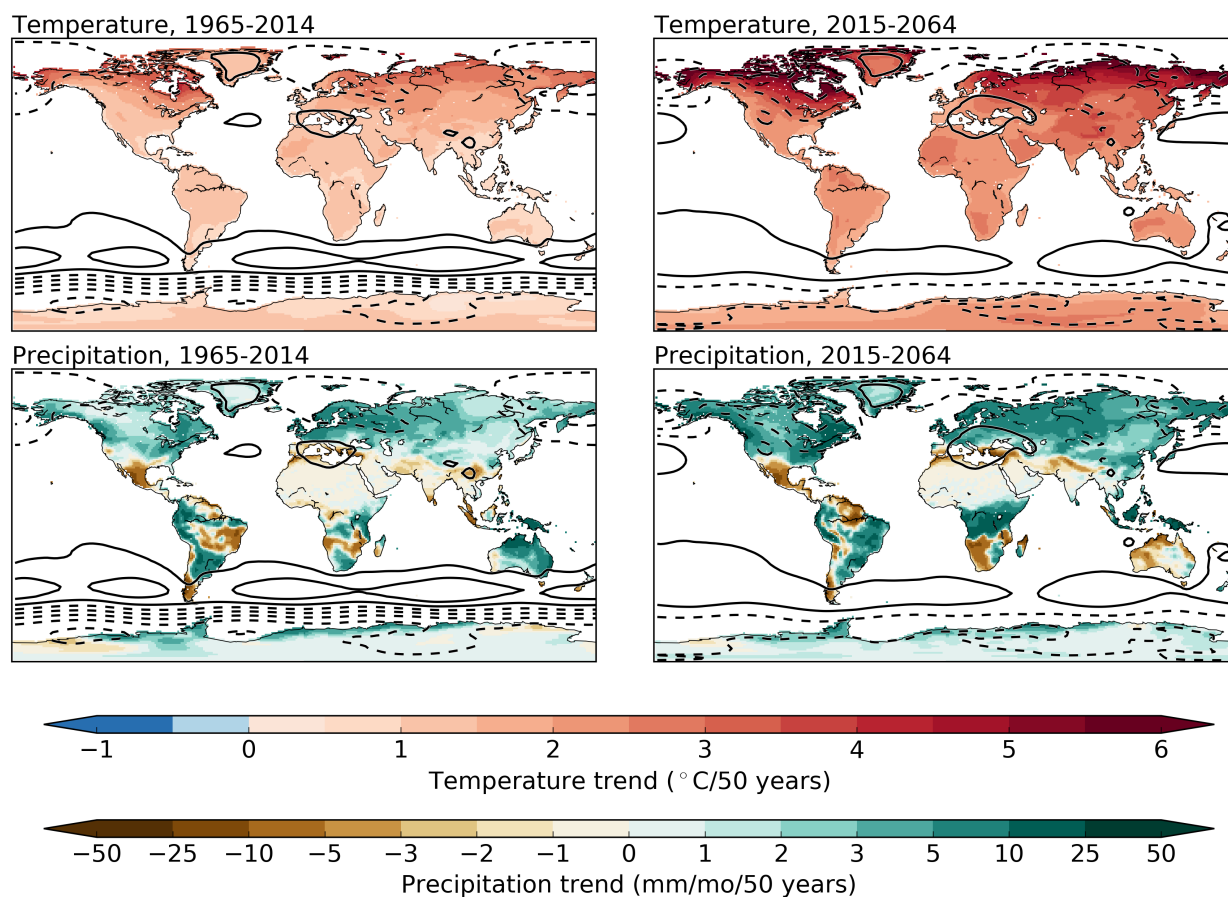


Figure S10: Ensemble-mean linear trends from 37 CMIP5 models in DJF temperature (top row) and precipitation (bottom row) for the past (left column, 1965-2014) and next (right column, 2015-2064) 50 years. Trends in SLP are indicated by contours, with a contour interval of 1hPa/50 years, beginning with contours of ± 0.5 hPa/50 years.

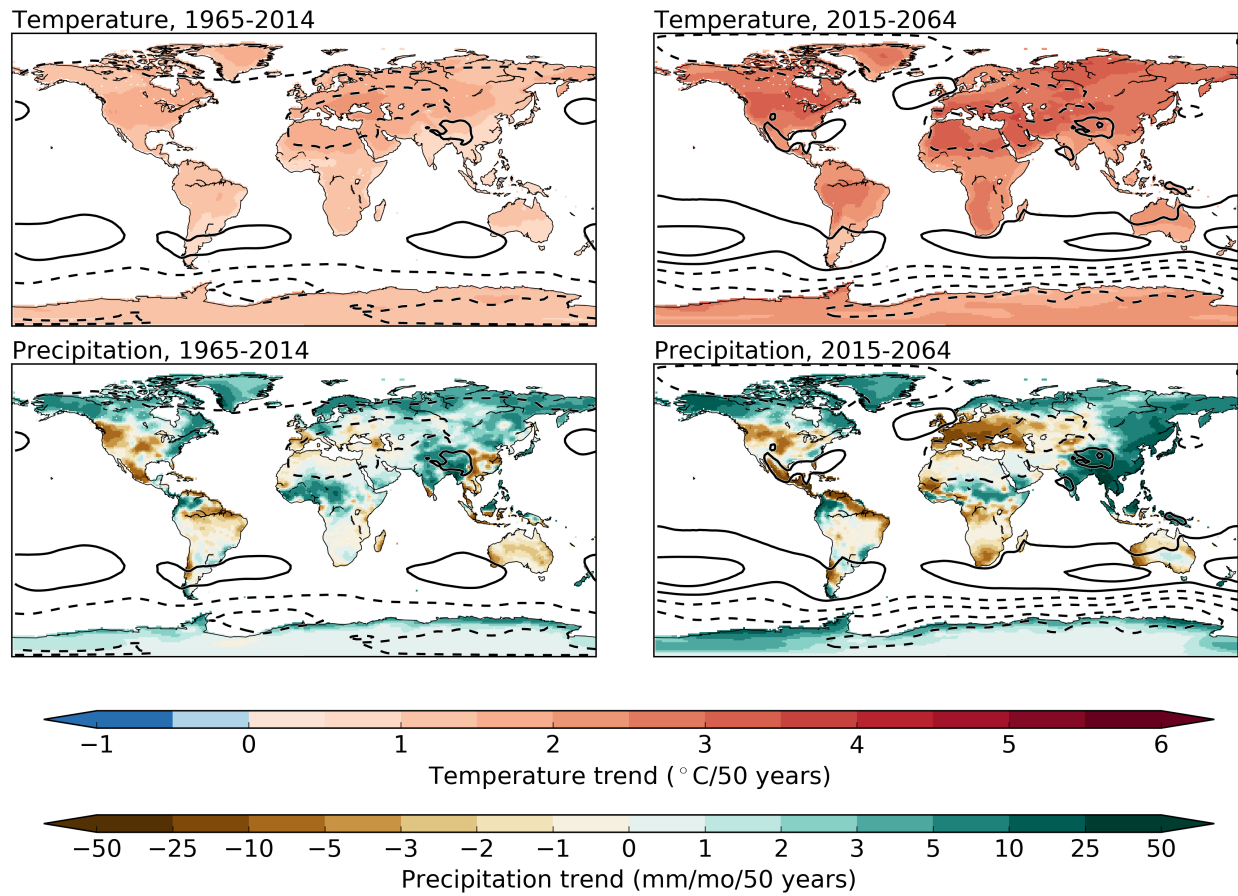


Figure S11: As in Fig. S10 but for JJA.

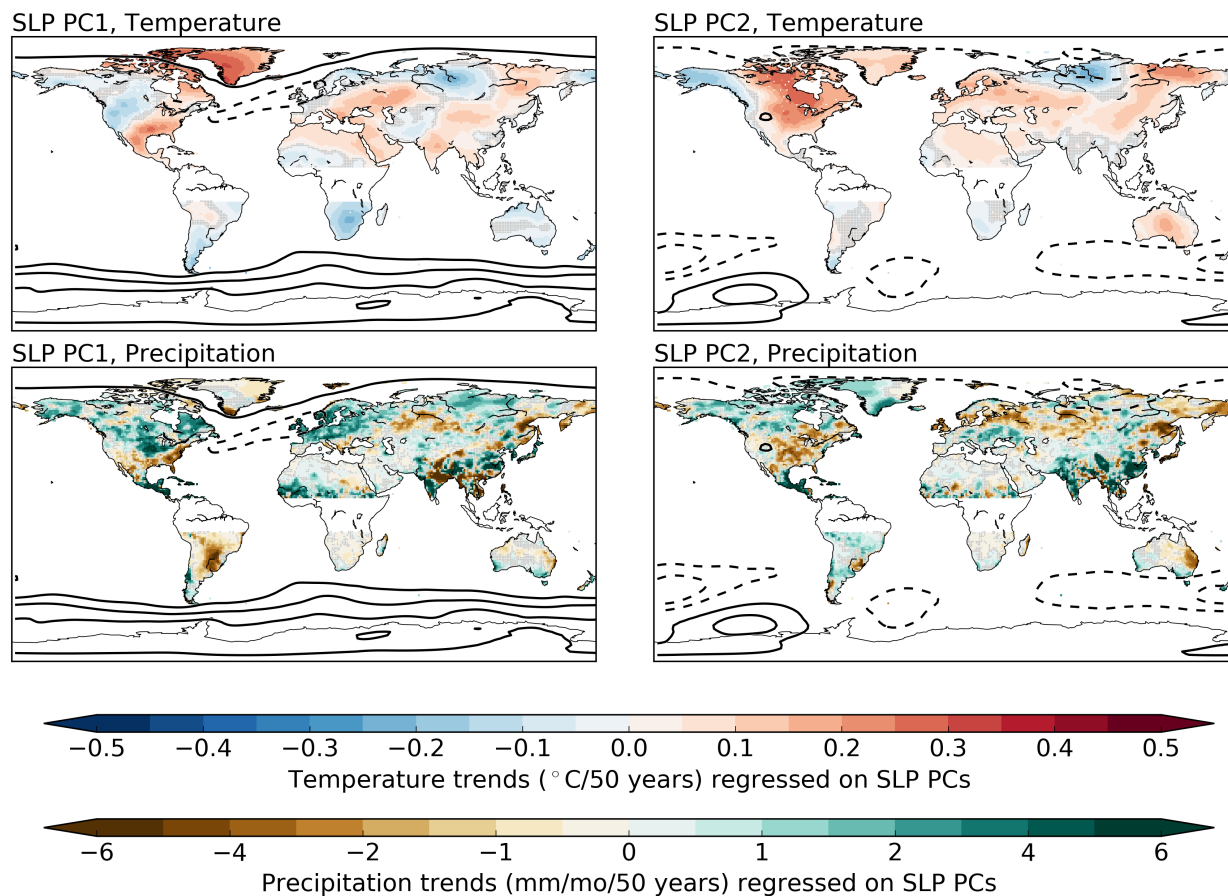


Figure S12: The regression maps of JJA temperature (top row), precipitation (bottom row), and SLP (contours) trends onto the first two normalized principal components of 50-year (1965-2014) JJA SLP trends across the Observational Large Ensemble. Contour interval is $0.5\text{hPa}/50$ years, and the zero contour is suppressed. SLP principal components are calculated separately for each hemisphere (poleward of 10°), but are shown on the same map for conciseness. The fraction of variance explained by the first two principal components is 17% and 12% in the Northern Hemisphere (41% and 12% in the Southern Hemisphere).

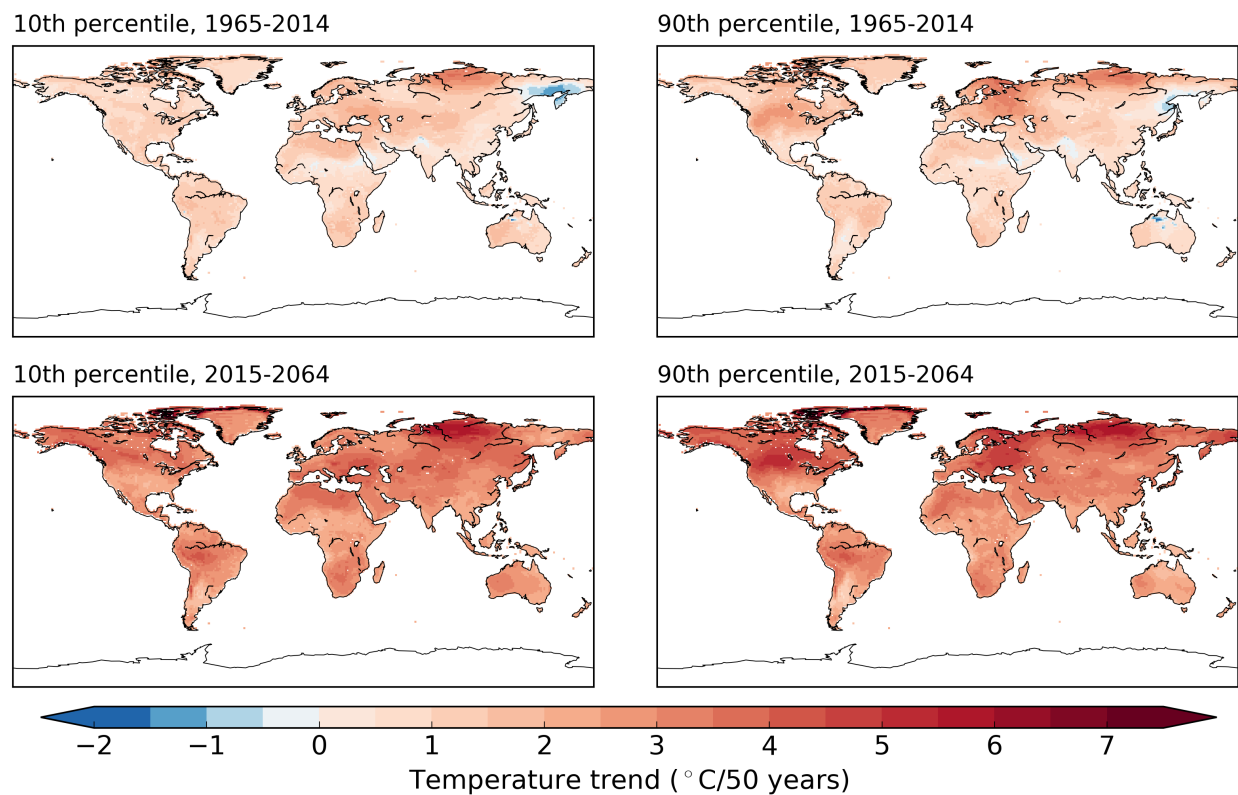


Figure S13: Range of 50-year JJA temperature trends from the Observational Large Ensemble for the (top) past (1965-2014) and (bottom) future (2015-2064). The left and right panels show the trend maps that accompany the 10th and 90th percentiles, respectively, of the NH extratropical (30-90N) land-average trends. The 10th and 90th percentile JJA temperature trends for the past (future) are $1.18^{\circ}\text{C}/50$ years and $1.53^{\circ}\text{C}/50$ years ($3.39^{\circ}\text{C}/50$ years and $3.74^{\circ}\text{C}/50$ years), respectively.

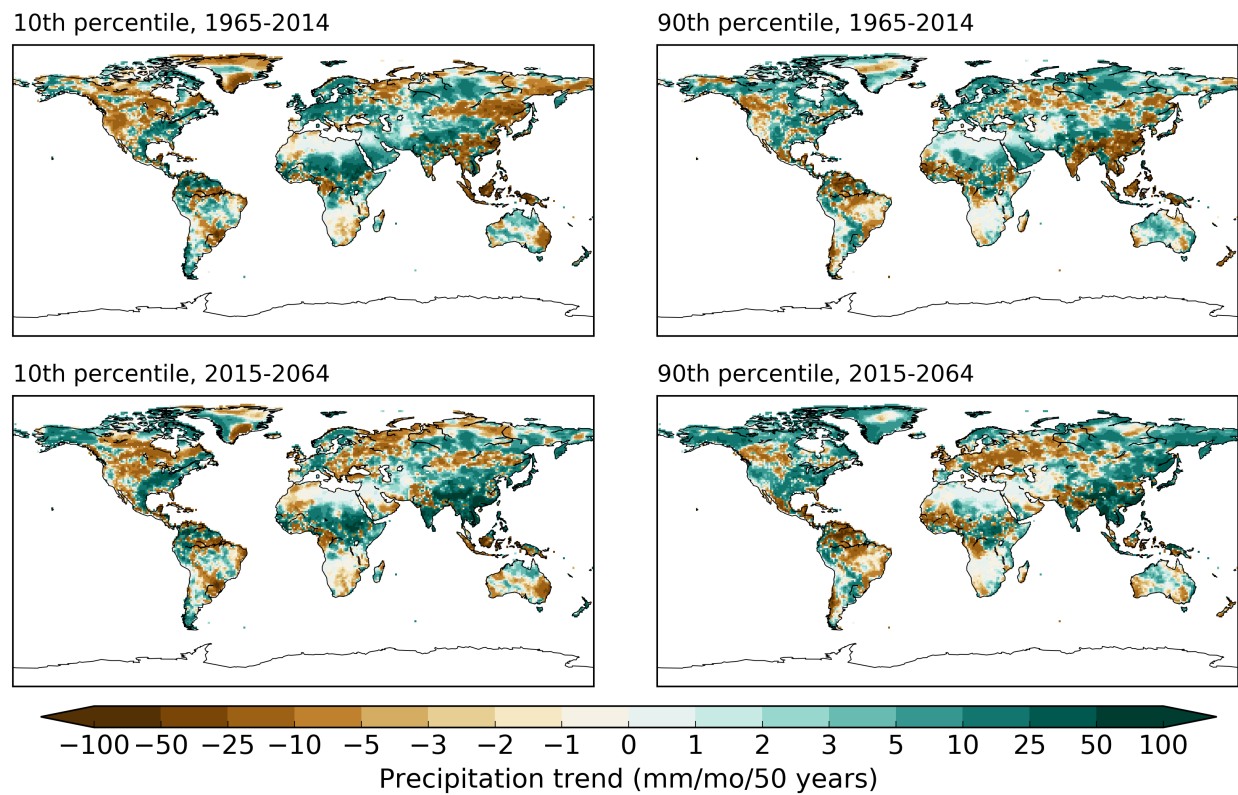


Figure S14: As in Fig. S13, but for precipitation. The 10th and 90th percentile Northern Hemisphere extratropical land JJA precipitation trends for the past (future) are 0.26 mm/mo/50 years and 2.56 mm/mo/50 years (2.27 mm/mo/50 years and 4.58 mm/mo/50 years), respectively.

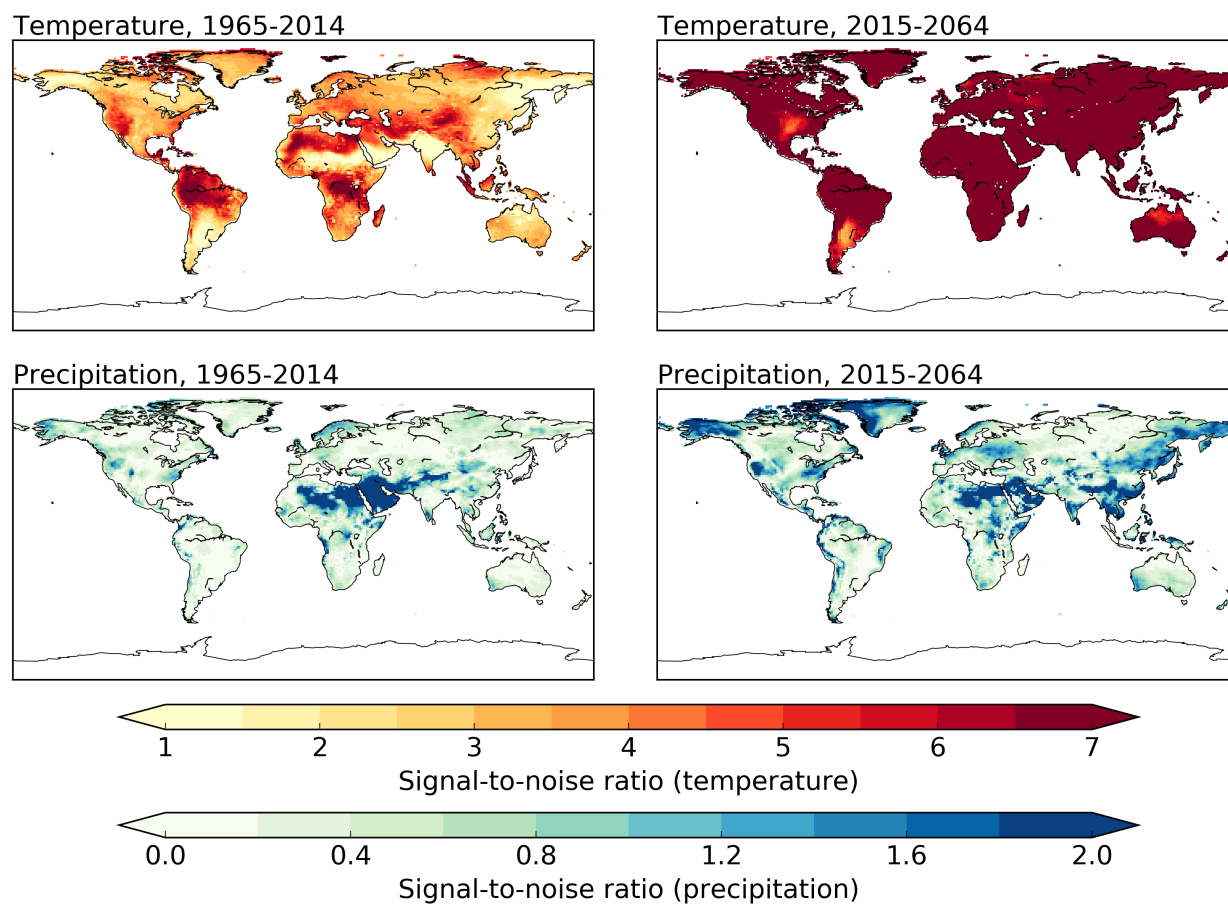


Figure S15: The signal to noise ratio (SNR) in the Observational Large Ensemble for 50-year trends in the past (left column, 1965-2014) and future (right column, 2015-2064) for JJA (first row) temperature and (second row) precipitation. SNR is estimated as the magnitude of the ensemble mean 50-year trend normalized by the standard deviation of trends across the ensemble.

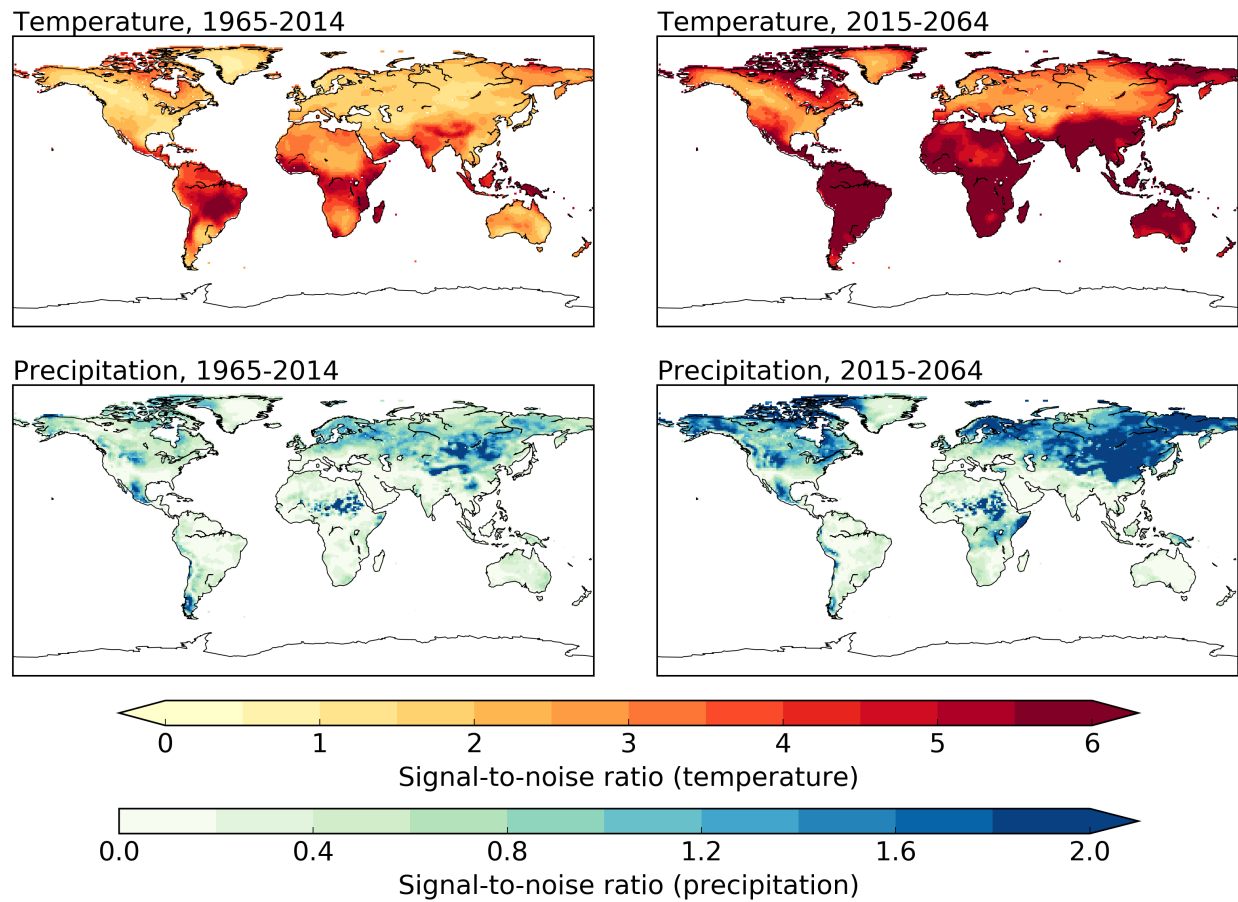


Figure S16: As in Fig. 12, but using the ensemble mean from 37 CMIP5 models as an estimate of the forced trend.

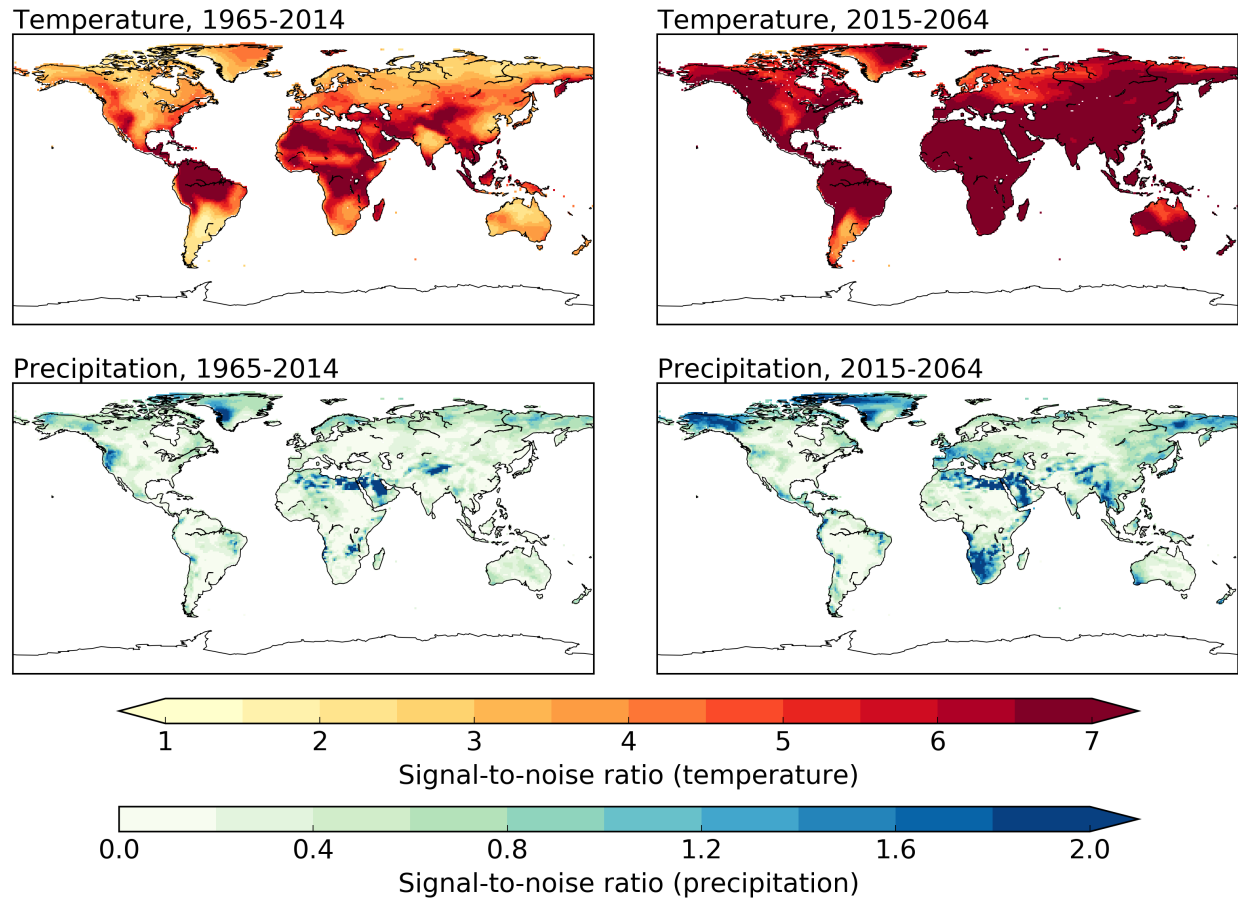


Figure S17: As in Fig. S16, but for JJA.